Fatigue short crack behaviour in the surface treated medium carbon steel

D. Kocańda and S. Kocańda

Military University of Technology, Faculty of Mechanical Engineering, Warsaw, Poland

ABSTRACT**:** *The aim of this paper is to provide the results of own researches into free short fatigue crack initiation and growth in residual stress field induced by surface laser hardening or by shot peening. Comparable study was carried out primary for non-treated medium carbon steel specimens in air and at room temperature. The high cycle fatigue tests were conducted under fully reversed torsion for smooth both non-treated and treated specimens. The paper consists of two parts: first part presents the experimental results of these studies whereas the second one derives the proposition of short crack growth description in the aspect of probabilistic approach.*

INTRODUCTION

Since over two last decades short fatigue crack behaviour has been intensely investigated in the aspect of learning both an early growth of fatigue crack and the nature of the fatigue resistance of engineering materials. Practical aspect of this study consists in estimation of the lifetime of the structures more precisely taking into account the short crack growth regime. Many studies have shown that a large proportion of the fatigue life of a component can be taken up in the development of short cracks depending on the applied stress level. Numerous papers and books have been published on the short crack behaviour in metallic structures and recently in advanced materials such as ceramics and intermetallics as well. The problem of short cracks, generally, has been widely presented in two exemplary books [1,2] and in the paper [3]. Comparative study due to the mechanism of cracking acting in traditional and advanced materials has been performed in [4].

The considerable interest into the research of the short cracks has been induced by so-called anomalous growth rates of these cracks near-threshold stress intensity factor. Short crack effect is associated with the fact that the growth rates of short cracks can exceed those ones of large cracks at the same applied stress intensity range ΔK. Small cracks can propagate at the applied stress intensities less than the value of fatigue threshold ΔK_{th} be-

longs to long cracks. Experimental studies carried out for various metallic materials distinguish two stages of fatigue short crack growth following the microstructurally and physically short crack growth. The differences in the crack behaviour that are specific for each stage of the crack growth were described in the mentioned references. Miller [5] has introduced three threshold values to fatigue crack propagation, one for a pure single crystal and two for a polycrystalline material. With respect to a polycrystalline material the first threshold value is related to the material microstructure (microstructurally-based threshold) and the second one is mechanically-based value. Threshold stress intensity factor K_{th} of linear fracture mechanics is referred to mechanically-based threshold and it differs short and long crack ranges. In the case of a pure single crystal the initiated crack, if the stress level is high enough, overcome the threshold barrier of the single crystal, represented possibly by a dislocation cell wall in the persistent slip bands ladder-like structure.

Many interesting considerations in terms of short crack growth have been provided recently. A review of crack closure, fatigue crack threshold and related phenomena were performed in [6]. Generally accepted closure concepts with particular reference to the roughness-induced closure, corrosion-induced closure and plasticity-induced closure were re-examined in Ref. [7]. Crack closure effect can play an important role in a crack propagation and has been used to explain several phenomena, like the influence of load ratio, load interaction, crack growth retardation with increasing crack length etc. [8] .

Behaviour of short crack growth in metallic material

In the literature related to the studies of early fatigue crack growth in the materials two terms of crack are treated equivalently, namely small and short cracks and a distinction between these cracks is not always clearly recognized. Halliday et al. [9] propose to define the small cracks as the cracks being of a size comparable to the grain size or to the scale of local crack tip plasticity. Small cracks are small both in depth and surface length. The propagation of small cracks is correlated with intrinsic stage I growth. In plain and polycrystalline specimens these cracks initiate mainly in the persistent slip bands in the favourably orientated grains to the τ_{max} plane and they have the growth strongly influenced on the grain boundaries. Short cracks need only be small in the direction of crack growth but can have long surface lengths. Short cracks of dimensions comparable to several grain sizes are called as microstructurally short cracks. As a consequence of crack interactions with the microstructural barriers (grain boundaries, non-metallic

inclusions, second phase precipitations) a high initial growth of those cracks is subjected to intermittent retardations and accelerations or event partial arresting at a transient length called as microstructurally-based threshold d_{th}

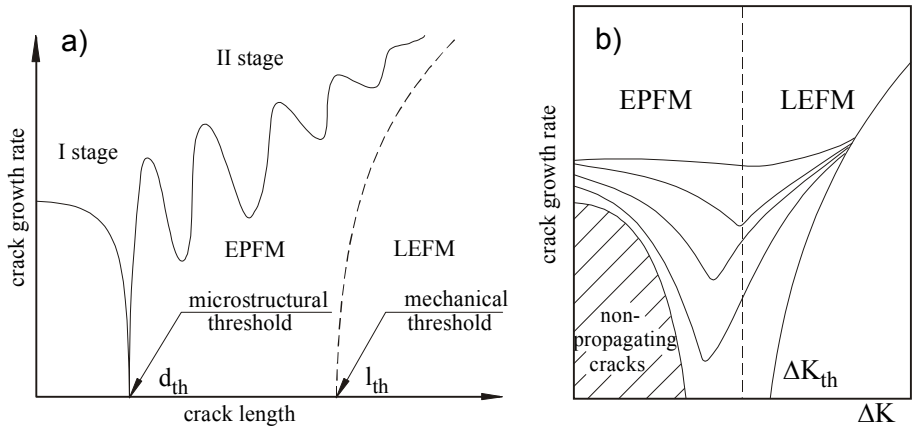

Figure 1: Schematic courses of crack growth rates against crack length (a) and stress intensity ΔK (b) in the range of short and long cracks; see text for explanation.

(Figure 1). This manner of growth explains abnormal behaviour of the microstructurally short cracks. High initial microstructurally short crack growth rates suggest the absence of closure effect at the beginning of their growth. It seems to be rationalized thinking because the small cracks have not previous plastic deformation zone along the crack lips. Decreasing trend of surface short crack growth rates can be caused rather by roughness than other forms of closure effect. It was found for a wide range of materials (low and medium carbon steel, high strength steel, aluminium alloy and titanium) that large decreases in crack growth rates are more pronounced in fine grained material than in coarse grained material [10]. This effect of microstructure on crack growth rate results from two causes: grain boundary (blocking of the plastic zone i.e. slip bands ahead of the crack tip at the grain boundary) and crack deflection when the crack runs across successive grains.

The transient crack differs the crystallographic stage I from the stage II of crack growth regimes. Physically small cracks of the length less than 1mm belong to the stage II of crack propagation. Monotonically increasing growth rates of those cracks show an oscillating pattern of growth with the

amplitude of the oscillations decreasing as the crack gets longer up to a transient length called as mechanically-based threshold l_{th} (Fig. 1). Microstructurally and physically short crack growth regimes are often commonly named as the short crack regime. The results of crack growth rate investigations indicate that for a wide range of polycrystalline materials (steels, aluminium alloys, titanium alloys) [9], [11] and for single crystals [11] [12] the intrinsic behaviour of physically short cracks is identical to that of long cracks. Crack growth tests give higher growth rates for physically short cracks than those observed for the long crack data at the same nominal ΔK ranges when the growth occurs below the ΔK_{th} value obtained for long cracks at the same R ratio.

Several reasons have been considered by the investigators to explain high rates of short crack growth and the differences between the growth of long and short cracks. Especially, both crystallographic grain orientation and large cyclic strain in the form of slip bands that are developed within the grains have been emphasised in promoting rapid growth of small cracks. It has been suggested that much reduced amount of crack closure below ΔK_{th} can explain their enhanced growth rates. Extensive studies of short and long crack growth rates, closure effect and crack profile has been developed for the aluminium 2024-T351 alloy under wide range of stress ratios R (R=0÷0.7) [9]. The results indicate that crack profile of free initiated crack is semicircular in 2024-T351. Threshold value ΔK_{th} is strongly dependent on R ratio and shows decreased tendency as a crack becomes shorter. For long cracks ΔK_{th} is lower for higher R. Value of stress intensity factor at crack closure K_{cl} increased from a value of 0.5 MPa$\sqrt{m}$ at crack length comparable to one grain size in 2024-T351 to the value of ≈2 MPa$\sqrt{m}$ near threshold (300 μm). For short cracks the magnitude of the closure stress was the greatest at the smallest crack size recorded and then decreased up to a crack length of about 0.5 mm. The cracks were closed over larger fractions of the fatigue life at smaller crack sizes (R=0÷0.1). It is seen that substantial amount of crack closure can be present during the growth of very small fatigue cracks at R≈0 and this needs to be taken into account when the early stage of crack growth is assessed. Short crack effect and closure dismisses at high load value and high R ratios. The crack growth behaviour of microscopically and physically short cracks is controlled by different crack tip plastic zone sizes and different friction stresses [13]. Taking these assumptions into account the short crack growth model has been proposed.

The fatigue crack growth analysis at notches may be divided into the stage of crack propagation through a notch plastic zone, through crack

propagation in a changing stress field and to long cracks in an elastic notch stress field. The development of small and short cracks at stress concentration field and the role of microstructure in this process are of essential importance for the fatigue life of such component as aero engine disc. The experimental results obtained for α titanium alloy IMI829 show that the growth rate of short fatigue cracks first increases and then decreases with crack growth. This stage of crack growth is sensitive to the microstructure (influence of boundaries of prior beta grains and α colony) [14]. For both plain and blunt notched specimens of a medium strength steel higher local strains at the notch root lead to shorter stage I mode II cracks. In notched specimen the local strain is controlled by the geometry of the notch i.e. shape and the depth and by the applied stress. The threshold condition is covered by the arrest of stage I cracks by microstructural barriers. Transition from the stage I to stage II takes place when crack changes from shear to the tensile mode [15]. It is occurred within the notch plastic zone. Crack growth rates within the notch plastic field are higher than would be expected from LEFM analyses.

The short survey of the works proves the developments of the studies of short crack behaviour both in experimental and conceptual aspects for the last years [16].

The aim of this paper is to provide the results of own researches into free short fatigue crack initiation and growth in residual stress field induced by surface laser hardening or by shot peening. Comparable study was carried out primary for non-treated medium carbon steel specimens in air and at room temperature. The high cycle fatigue tests were conducted under fully reversed torsion for smooth both non-treated and treated specimens. The paper consists of two parts: first part presents the experimental results of these studies whereas the second one derives the proposition of short crack growth description.

SHORT CRACK BEHAVIOUR IN MEDIUM CARBON STEEL

Short crack behaviour in the normalised 0.45% carbon steel

A normalised medium carbon steel 45 of ferrite-pearlite structure and of composition (wt. %): 0.48 C, 0.66 Mn, 0.24 Si, 0.02 P, 0.019 S, 0.25 Cu, 0.24 Cr, 0.028 Al, 0.03 Mo, remainder ferrite was used for the fatigue tests. Mechanical properties of the steel were as follows: yield stress = 425 MPa, ultimate tensile stress = 690 MPa, elongation = 18 %, reduction of area = 40 %. Hour glass shaped specimens of geometry given in Figure 2 were

finely polished first by successively finer grades of emery papers and then by a diamond paste to 10 μm or 1 μm. Prior to fatigue test the sample gauge was lightly etched in 0.5 % nital to reveal microstructural barriers for crack advance. Torsion tests were carried out under load controlled reversed torsion at 5 Hz of frequency. Surface crack growth was monitored by taking the plastic replicas from the specimen surface at given intervals of load cycles N_i. Crack length and crack population in an unitary area were estimated with the help of an optical microscope equipped with a computer image analysing system. The spots of crack initiation and characteristic features of surface short crack growth were established on the basis of further observations on the replicas made with the help of a transmission electron micro-

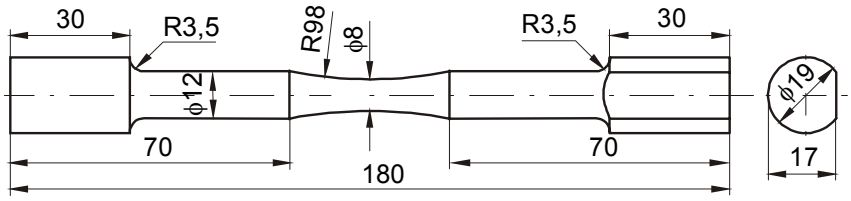

Figure 2: Geometry of specimens; dimensions in mm.

scope (TEM). For the micro-observations carried out with the TEM the replicas were shadowed by platinum.

Crack initiation and growth

Free surface small cracks in the normalised carbon steels, 45 steel included, nucleate usually in persistent slip bands formed in ferrite grains and propagate practically through these grains. An average size of ferrite grains was 15-25 μm. A network of the surface microcracks nearly perpendicular to each other is originated with the specimen-axis-orientated cracks prevailing. This is resulted from the ferrite bands originated while rolling bars. Examples of crack initiation and propagation within ferrite are shown on the micrographs in Figure 3. The images have been derived from the sample surfaces under examination at $\tau_a = 230$ MPa after $4 \cdot 10^3$ cycles. Figure 3a shows an individual microcrack of a length10 μm grown in the slip plane inside the ferrite grain. Three microcracks perpendicular to each other are shown in Figure 3b. These microcracks are mutually blocked by previously initiated cracks. Strongly developed slip bands even with visible slip lines are seen in Figure 3c. There is the site of crack initiation in the slip band bordered with a pearlite grain boundary. Parallel cracks shown in Figure 3d are become

visible in slip bands as well, with well-marked extrusions. Examinations indicate typical behaviour of surface shear cracks such as temporary arrest at the ferrite grain boundaries and most often longer arrest at pearlite grain boundaries [17].

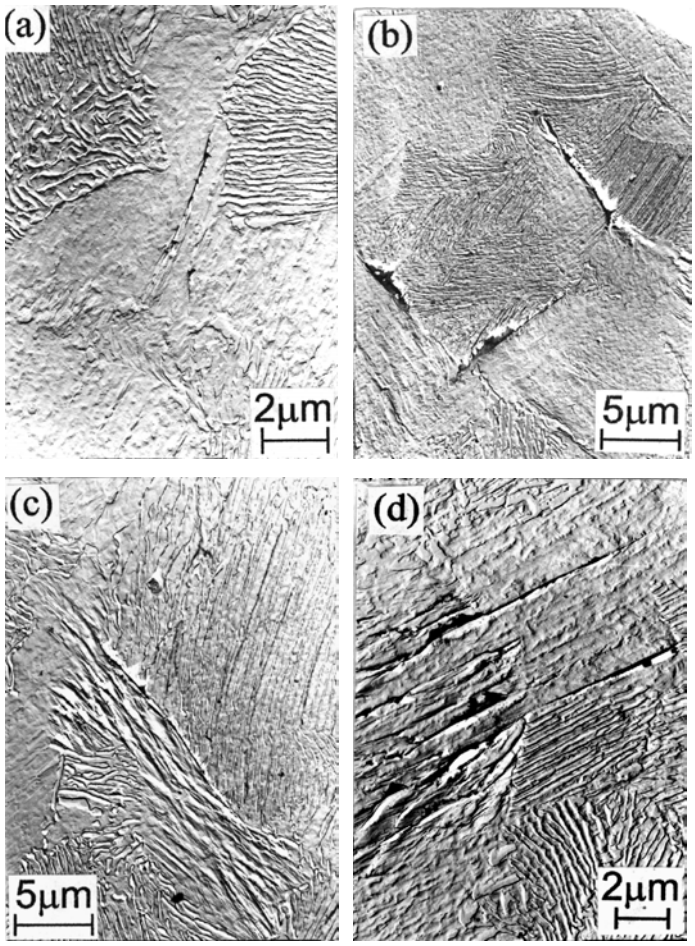

Figure 3: Systems of surface short cracks in a normalised specimen; see text for explanation.

This crack arrest at pearlite grain boundaries is consisted in finishing intrinsic stage I regime. Stage I shear crack growth involves about 10 ferrite grains (150-200 μm) and then stage I-like regime is observed up to the greatest drop of growth rates at the length of 400 μm which is coincided with reaching a boundary of pearlite grains colony by running crack. Stage

I-like regime is attributed to the slowest crack growth rate of about 10^{-8} m/cycle, and probably, to the development of local plasticity and crack closure particularly in compressive part of cycle (R=-1). Considerable fall is observed at the lowest stress level under examinations (τ_a = 164 MPa) below the fatigue life of material (τ_{fl} = 168 MPa) and it is referred to non-propagating crack. Depend on the applied stress levels either the stage I or stage I-like regimes can take 50-80% of the lifetime of materials. Afterwards, the stage II of physically short crack propagation takes place. Surface crack growth behaviour in the regime II is identical to that of long cracks. In the stage of long crack the crack paths deflect at the angle of a round 45^0 to the specimen axis and then the branched cracks run in two mutually perpendicular directions of maximum normal stresses.

The curves on Figure 4 reflect short crack passing the microstructural barriers at various intensities depend on the applied stress. Irregular increase of short crack lengths and crack growth rate variations against cycle ratio N_i/N_f (N_i – current number of cycles, N_f - number cycles to failure) are performed on the Figure 4a and 4b, respectively. Various paths of surface short crack propagation are attributed to local changes in the growth direction of crack depth. The evidence of this fact is reflected on the TEM micrograph

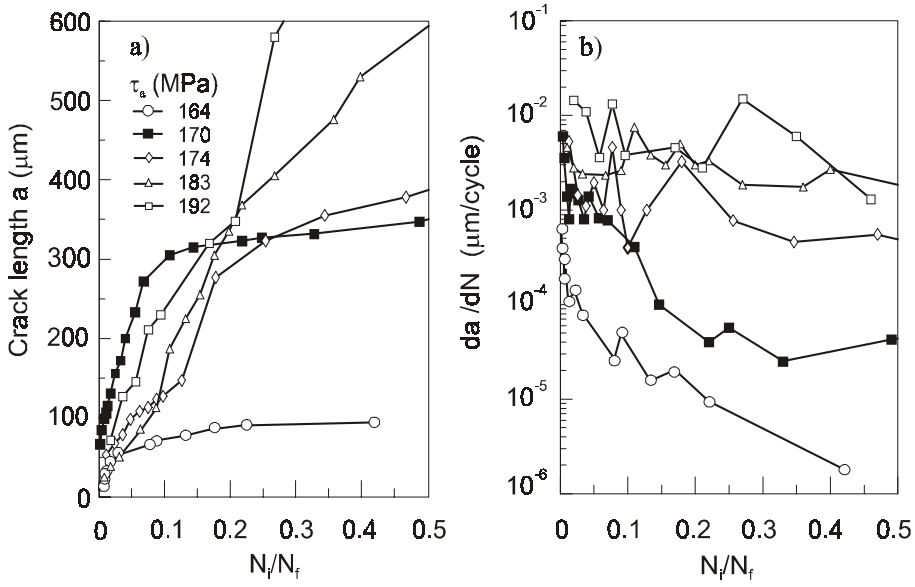

Figure 4: Plots of short crack lengths (a) and crack growth rates (b) against cycle ratio N_i/N_f drawn for the normalised specimens tested under different shear stress amplitudes τ_a .

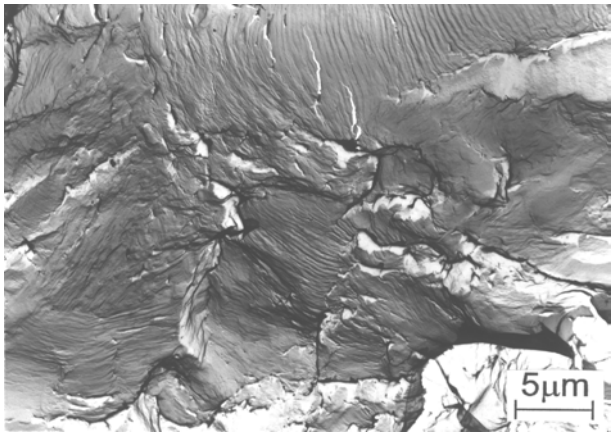

Figure 5: TEM micrograph of the fracture surface with the systems of variously orientated fatigue striations.

of the fracture surface shown in Figure 5. Certain systems of variously orientated plastic fatigue striations seemed there in a small area of fracture surface (15µm x 15 µm) indicate four directions of crack depth growth.

Crack density

Characteristic feature of surface microcracks is their great density in unitary area. Great density of microcracks formed in early stage of fatigue process proves a necessity to consider it in the models of short crack growth description and fatigue life estimation [16]. The plots in Figure 6 show significant fluctuation of crack population as function of cycle ratio. Here should be emphasized the share of crack coalescence process in reduction of the crack density. Due to these curves lower crack density and any saturation stage of it is observed in the samples tested under lower stress levels (τ_a = 164, 170, 174 MPa). At higher applied stress (τ_a = 183, 192 MPa) the density of cracks has achieved maximum value and then decreased because of crack coalescence.

Dynamic of crack propagation and coalescence process can be watched with the help of the exemplary column diagram (Figure 7). Cracks less than 20 µm were disregarded in the diagram. A great regularity of crack density there was found in the range of crack length 50-100 µm with increasing cycle ratio. In the case of crack length greater than 100 µm an increase of generally small crack density is seen in the range of 0-0.5 N_i /N_f. In further stage of fatigue process the variation of crack density is connected with new

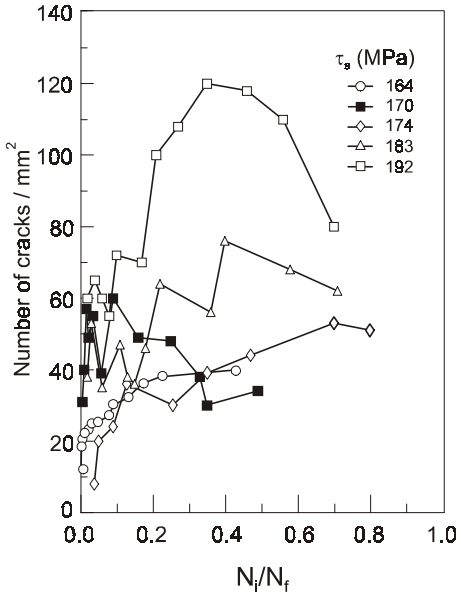

Figure 6: Short crack population against cycle ratio in the normalised specimens tested under different shear stress amplitudes τ_a .

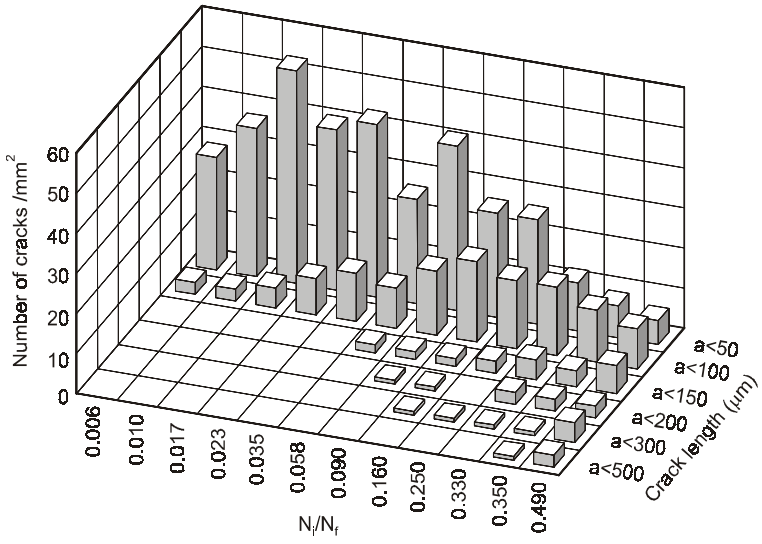

Figure 7: Distribution of crack length counted for the specimens tested at shear stress τ_a =170 MPa.

created cracks and cracks joining alternatively. At higher applied stress (τ_a = 183 MPa) cracks initiation activity begins early since 1-3 % of cycles to failure, cracks grow faster and process of crack coalescence runs speeder. The consequence of those circumstances is a greater variation of crack density and the zigzaggy courses of plots in Figure 6.

SHORT CRACK BEHAVIOUR IN THE SURFACE TREATED 0.45% CARBON STEEL

Surface treatment methods used in order to extend the lives and fatigue properties of structural components have been recognized for many centuries. However, such treatments are now an integral part of manufacturing of structural components in many industrial applications such as automotive components, gear wheels, mining machinery, aerospace engineering and so on. These treatments generate a beneficial residual stresses in the surface layer that are induced, for example, by phase changes, mechanical plastic surface deformation or chemical means. The use of these methods in particular applications is highly dependent on reliability of this process and ensuring that the treatment does not lead to surface damage i.e. does not generate cracking which develops from local stress concentrators (initial inclusions, melting spots or severe surface roughness). In many cases of using surface treatments significant improvements in fatigue life can be obtained. However, in each case of working component the fatigue crack can be initiated and can propagate slower or speeder depends on many factors.

Generally, compressive residual stresses present in the near surface layer increases the time to crack initiation and decreases fatigue crack growth rate, particularly in the earlier stages of growth. It means that the residual stresses increase the level of crack opening stress [18]. Early stage of crack growth is related to short crack propagation, and therefore, the microstructure, surface distortion and thermomechanical state of the material play significant role in crack growth behaviour. Crack density and the speed of crack coalescence are the successive factories which decide of durability of the treated components. Compressive residual stresses retard the process of crack coalescence in the range of short cracks. This fact results in increasing the life of component. It should be emphasised that surface treatment brings benefit mainly in the range of short cracks. Depends on the effectiveness of used method the short crack range can take from 80% to 90% of total life of the component. If the cracks become long the surface treatment has no meaning. Explanation of the benefit that the treatment brings to fatigue re-

sistance can be found on the way of learning the phenomena which are characteristic for each method.

Short crack behaviour in laser treated specimens

Experimental procedure

Surface laser treatment is often used for improving the fatigue strength of machine parts, and so the fatigue properties of laser hardened components are the subjects of numerous works. However, studies of crack initiation and the rate of crack growth in these components are only reported in a few references [19], [20]. Particularly, the problem of short crack growth is seldom discussed but the works [21] and [22] provide some results of short crack behaviour in laser hardened medium carbon steel under reversed torsion.

For the study hour glass shaped specimens of the normalised 0.45% carbon steel of composition, mechanical properties and the dimensions given earlier, have been surface treated by a 1.5 kW power continuous wave CO_2 laser in a nitrogen-oxygen atmosphere at room temperature. The laser beam velocity was equal to 20 mm/s. The specimen surface was covered by laser tracks of 3.5 mm width in two different manners: circumferentially with a stroke of 3.5 mm (Figure 8a) or with a fully hardened gauge surface by overlapping tracks (Figure 8b).

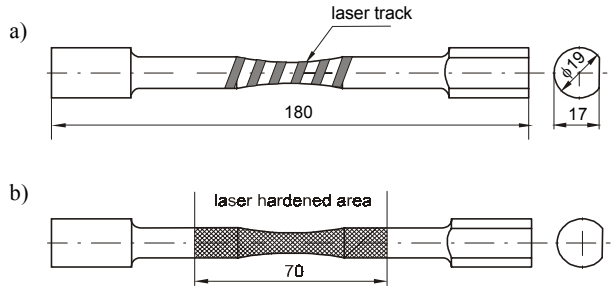

Figure 8: Two manners of surface laser treatments applied for the specimens: by circumferential tracks (a) or with a fully hardened gauge surface with overlapping tracks (b).

The depth of the hardened layer (of semi-elliptical shape) was about 1 mm. The gauge surface of the specimens were not polished but lightly etched prior the fatigue tests. Analysis of the structure of hardened zone revealed a narrow, lath martensite in the surface layer and a martensitic-bainitic mixture at the bottom of the laser track. The surface microhardness of the

treated specimens was equalled to 650 μHV_{100}, the microhardness of the matrix was 170 μHV_{100}. Surface residual stresses were measured by the X-ray method. Compressive residual stresses of value 600 MPa were measured in the laser tracks and a round 250-300 MPa in the matrix between the tracks. The samples have been subjected to reversed torsion. Surface crack growth was monitored using the replication method. The TEM facility was used both to locate short cracks and to reveal characteristic features of crack initiation and propagation in the examined specimens. For the TEM analyses the replicas were shadowed by platinum.

Crack initiation and growth

In the specimens circumferentially treated the fatigue cracks were found to initiate almost exclusively in slip bands formed in the ferrite grains of the matrix between the laser tracks only. In the tracks themselves no nucleated cracks were observed. The TEM analyses of the replicas taken from the specimen surface proved that in very early stage of life (0-0.15 N_f) several shear cracks initiated inside separate ferrite grains. Probably, the surface compressive stresses that are present between the laser tracks affect against joining the small cracks. It means the stage I growth runs only inside the ferrite grains. The external strain energy produces persistent slip bands in

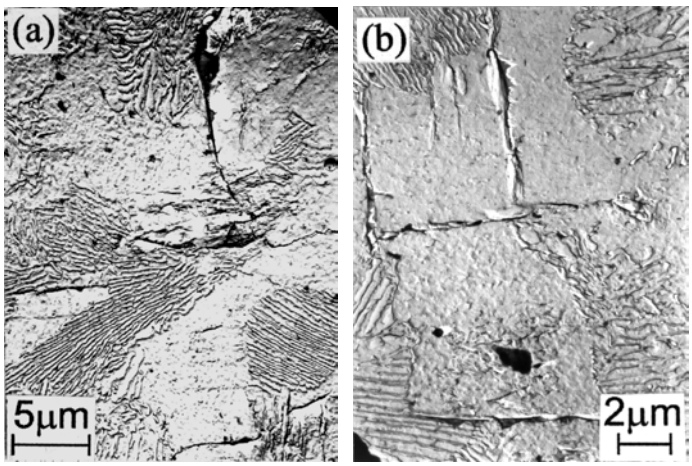

Figure 9: Different systems of surface short cracks; see text for explanation.

successive ferrite grains and a net of shear cracks initiated there. Afterwards, those small cracks join the shear cracks in adjacent grains in stage I-like growth. Surface small crack growth patterns were observed on speci-

men tested under a shear stress amplitude τ_a = 192 MPa after $2 \cdot 10^4$ cycles (Figure 9a) and after $2{,}1 \cdot 10^5$ cycles (Figure 9b) ($N_f = 3 \cdot 10^5$ cycles). Privilege direction of those crack growths is the direction parallel to the specimen axis (Figure 10a). In a vicinity of the laser tracks the long cracks branched at nearly a 45^o angle to the sample axis and advanced on in direction of maximum normal stresses. Cracks were completely arrested at the border of the laser tracks and did not enter the tracks. Either the structure of laser track or compressive residual stresses acted there constituted a strong barrier for the cracks. The failure crack propagated along the border of the track (Figure 10b). The images have been derived from the samples tested under a shear stress amplitude τ_a = 196 MPa after $1{,}9 \cdot 10^5$ cycles. Number of cycles to failure was $N_f = 2{,}05 \cdot 10^5$ cycles.

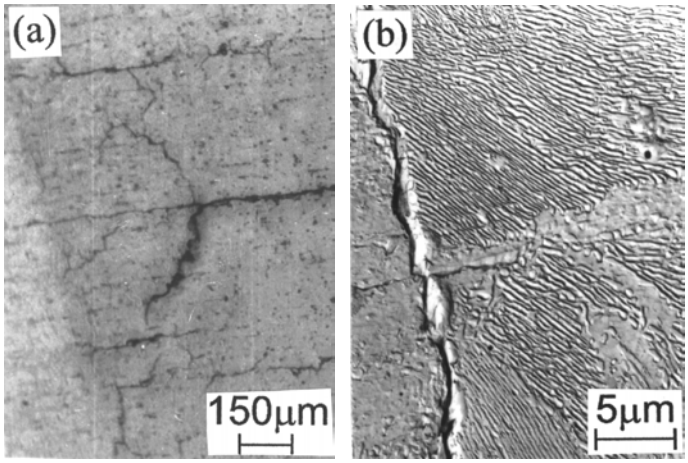

Figure 10: Optical graph of the specimen surface derived from a vicinity of the hardened zone (seen on the left part of the graph) and the matrix (a), TEM micrograph derived from the border between the hardened zone and the matrix (b).

Examinations of fracture faces with the help of a SEM derived additional proofs of cracking process running in the specimens. The micrographs shown in Figures 11a and 11b illustrate the mechanism of cracking within the track in the circumferentially treated samples. The lower plastic strain of the laser track and great stress differences between the matrix and the track help resist crack propagation through the track. Hence, the crack by-passes the laser track section with a change in growth directions below the track.

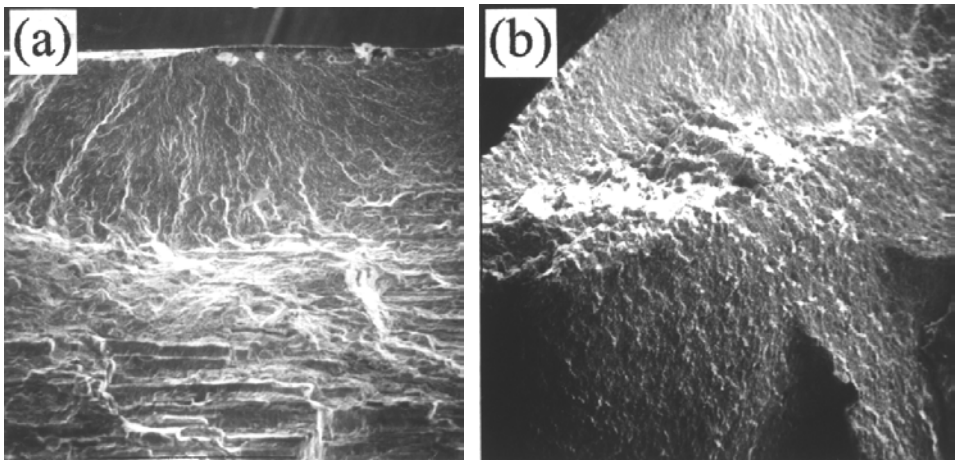

Figure 11: SEM micrographs illustrate the mechanism of cracking within the track in the circumferentially treated samples (a, b).

Complex mechanism of fracture in the examined specimens was established from TEM micrographs taken from different zones of fracture surfaces. A mixed brittle fracture, partly along grain boundaries and partly along cleavage planes, was found in the martensite structure of the surface layer of the laser track (Figure 12a). In the martensitic-bainitic structure, towards the bottom of the track, evidence of quasi-cleavage fracture with limited plastic deformation symptoms was found (Figure 12b). The micrograph of Figure 12c was obtained from the border zone between the hardened layer of the martensitic-ferritic structure and the matrix of ferrite-pearlite structure. Fatigue striations were only observed in the matrix below the hardened zone which are evident on Figure 12d.

The plots in Figure 13 reflect the crack growth rate behaviour in the discussed specimens that were tested under different shear stress amplitudes τ_a. The characteristics of crack growth rates as the function of crack advance and cycle ratio N_i / N_f are presented in Figures 13a and 13b, respectively. Continuous lines that joint the black marks represent experimental results whereas the dashed lines and white marks the calculated ones. The curves plotted in Figure 13 refer to crack advance in the samples with circumferentially hardened surface, except the plots signed as NL and FL that present the cracks grown in non-treated specimen and in the specimen with a fully hardened gauge surface, respectively. Behaviour of microstructural short cracks grown in the stage I-like was typical being temporarily arrested at the grain boundaries of both the ferrite and the pearlite. The fall of their growth

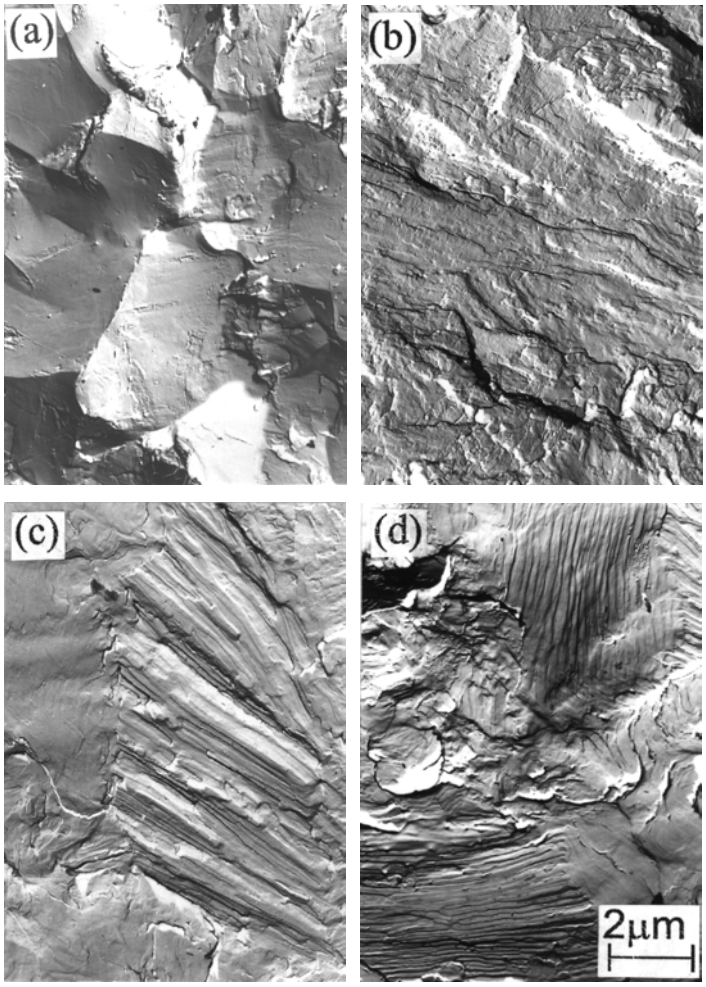

Figure 12: TEM micrographs of the surface fracture derived from the hardened layer (a, b) and the border zone between the hardened layer and the matrix (c, d).

rates was less and the growth was significantly slower than in the case of those cracks developed in non-treated specimen NL at the same load conditions. In the samples signed as L1, L2, L3 the stage I-like short crack growth regime is found to extend until the crack length a round 200 ÷ 300 μm. It corresponds to 15-20% fatigue life of the examined specimens. A comparison of the curves plotted for the cracks that were developed in non-treated specimens (NL) with those for the treated ones (L1, L2, L3) makes it evident that the short crack growth regime which includes the microstructurally

and physically short cracks growth regimes has been lengthened in duration for the hardened samples to 70-80% of the lives. This is due to the compressive residual stresses both in the laser tracks and in the zones between them, and from the limited plastic deformation around and ahead of the crack tip. Numerical analyses of crack growth behaviour through a compressive residual stress field indicate the increase of stress level of crack-tip-opening and decreasing of crack closure stress [18]. It means that crack tip is closed for longer time and the crack propagation period is lengthened in time. On the other hand, the authors of the mentioned work conclude, that the crack closure behaviour through a compressive residual stress field is very complicated and is influenced by the location of the crack tip.

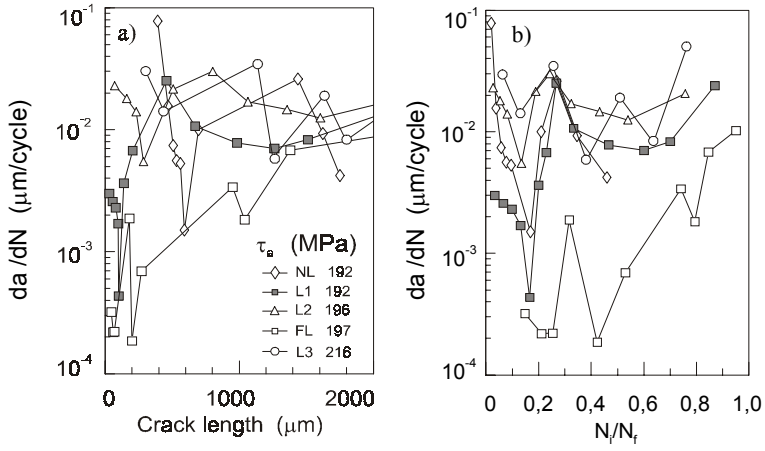

Figure 13: Experimental plots of crack growth rates against crack length (a) and cycle ratio N_i/N_f (b) in the laser hardened specimens tested under different shear stress amplitudes τ_a.

Another images of crack growth were observed in the samples with a fully hardened gauge surface caused by overlapping tracks. First of all, no short crack behaviour was observed in these specimens. Individual surface cracks were initiated in randomly distributed melted spots. Crack initiation activity began since 15-20% of total life it means the crack nucleation period was 5÷7 times longer than this one in the circumferentially hardened specimens. The SEM analyses of fracture surfaces proved that cracking process was running dynamically below and inside the laser track, and therefore, was invisible for longer time on the specimen surface. After passing the laser track the tensile cracks began to advance rapidly on the surface in two directions forming mutually crossing systems that are related to direc-

tions of maximum normal stresses. In these specimens much longer durability and lower crack growth rates were observed in a comparison with the circumferentially treated samples. It can be linked to a higher compressive residual stresses acted in homogeneously hardened surface layer.

Crack density

Experimental results revealed a great density of short cracks per unit surface area in the narrow non-hardened bands between the laser tracks (Figure 14). A maximum value of crack density of 160 cracks/mm^2 was counted in treated specimen L1. In this specimen the crack density was greater than this one counted in non-treated specimen NL tested at the same shear stress amplitude. A greater crack density was observed in the samples tested at lower stress. A saturation stage was achieved earlier at lower stresses than at higher ones. An increase in stress amplitude led to a decrease in crack density because of a faster crack coalescence process.

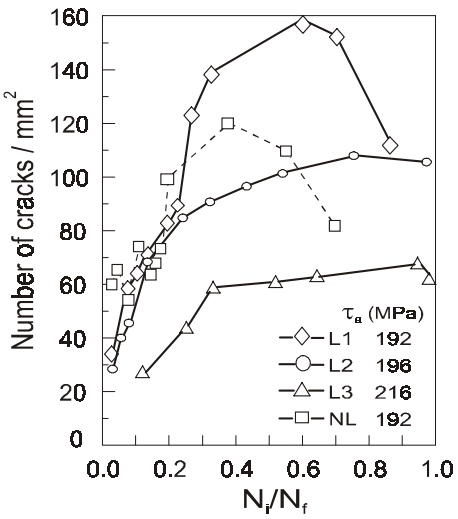

Figure 14: Short crack population against cycle ratio formed in the laser hardened specimens tested under different shear stress amplitudes; see text for explanation.

Distribution of surface crack lengths in the circumferentially treated sample (τ_a = 196 MPa) against cycle ratio N_i/N_f shows the exemplary column diagram in Figure 15. There may be found any regularity in crack density with an increase of cycle ratio. In the mentioned samples the microcracks initiation activity begins since 1÷3% of lives. Great density of microcracks

formed in early stage of fatigue process proves a necessity to improve the prediction of fatigue life of machine parts.

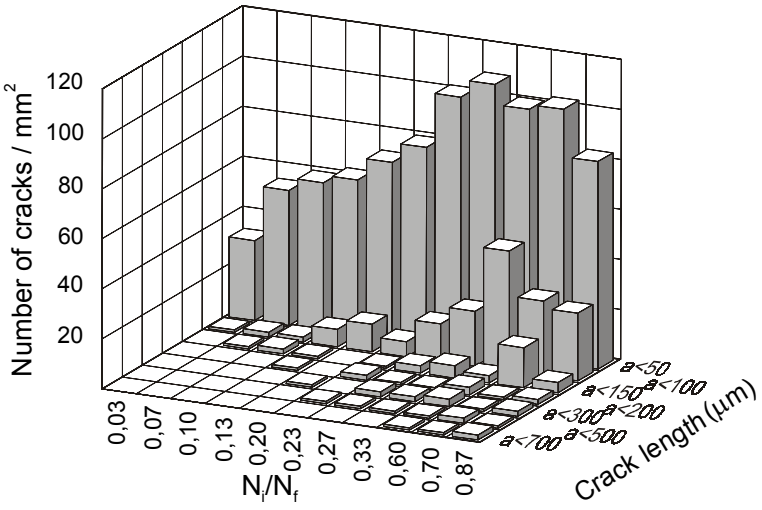

Figure 15: Distribution of crack length against cycle ratio N_i/N_f found in the circumferentially treated specimen tested at the shear stress amplitude τ_a = 196 MPa.

Summary

The studies of short crack growth behaviour in the circumferentially laser treated specimens made of a normalised medium carbon steel indicate that either high compressive stresses induced in the laser tracks or slightly lower stresses acted in the zones between the tracks as well as the type of loading (R= -1) lead to many characteristic phenomenon like as:

- stage-I short crack growth is limited to the ferrite grain boundaries,
- stage I-like short crack growth perform successive accelerations and retardations of crack growth rates that are resulted from the effect of material microstructural barriers. This crack growth regime has been shortened in crack length range in laser treated specimens in a comparison with this one found in non-treated specimens,
- transition from stage I-like crack growth to stage II one takes place at 20% of specimen fatigue lives independently on the applied stresses. Stage II crack growth is related to the physically short cracks and this regime was lengthened in laser treated specimens up to a round 70-80% of fatigue life. The growth rates of those cracks were speeder than growth rates of long cracks,

- generally, after this treatment the growth rates in each stage of crack growths were significantly lower and the fatigue lives were 1.5÷5 times longer than in non-treated specimens at all applied stresses of examinations,
- a great density of microcracks formed in early stage of fatigue process, on the one hand, and slower crack coalescence process, on the other hand, is characteristic for the laser treatment and leads to fatigue resistance in this stage of fatigue. Therefore, these phenomena prove a necessity to improve the prediction of fatigue life of machine parts.

Short crack behaviour in shot peened 0.45% carbon steel

Shot peening is used for structural components worked at a wide range of stress levels and designed for long fatigue lives. This treatment, being a surface cold working process, increases also fatigue resistance of components by introducing a beneficial compressive stresses in the near surface layer as well as additional effects such as grain refinement and grain sqeezing, phase transformations of the material, work hardening [23]. However, the life improvement is very dependent on the conditions of peening process. Peening benefit should be considered in two aspects: decreasing in fatigue crack growth rate and surface damage of components. The numerous reports note that peening increases the fatigue life and decreases the fatigue crack growth rate. Compressive stresses induced in the plastically deformed surface layer increase the crack opening stress thus reducing ΔK_{eff} and the crack growth rate.

On the other side, peening process generates the severe roughness and can lead to surface damage developing cracks. Surface roughness reduces the opportunity to detect cracks in early stage of fatigue process developing in the components because of surface distorsion. New approaches both to improvement of peening effect and to reducing the surface roughness become available in recent years. Two promising methods of surface working – laser shock peening and low plasticity burnishing are applied to life recovery in the aluminium alloy aircraft structure [24].

Experimental procedure

Normalised 0.45% carbon steel specimens of geometry shown in Figure 2 were pneumatically peened by steel shots of 0.6 mm diameter for 80 s at an air pressure of 0.6 MPa, giving an Almen intensity I = 0.39 A (mm). The coverage obtained was 200 %. Additionally, a double peening by glass shots of 30÷50 μm diameter was applied for a few samples in order to reduce the surface roughness induced by the singular treatment. The depth of the hard-

ened layer was in the range of 0.1-0.2 mm and the specimen surface microhardness was equal to 300 μHV_{100}. The microhardness of the matrix material was 200 μHV_{100} while the mean surface roughness R_a, was 1.52 μm and the maximum depth of roughness R_m = 14.76 μm.
Compressive residual stresses of values 250-320 MPa were measured in the surface layer of specimens by the X-ray method. The fatigue tests were carried out under reversed torsion in similar conditions as in the case of laser treated samples. The spots of crack initiation and characteristic features of short crack growth in the shot peened samples were established on the basis of the SEM and TEM observations on the replicas and also on microsections of the specimens. The results of the study in short crack behaviour in the peened specimens are the subjects of the works [25], [26].

Crack initiation and growth
In a surface layer that exhibits strong plastic deformation due to peening, the exact positioning of the sites of crack initiation is difficult. Both the grain boundaries and the slip bands are not visible in the surface layer. In peened specimens the structure of the surface layer differs markedly from that of a non-treated sample. Figures 16a and 16b show the structures of the plastically deformed layer on a longitudinal section, parallel to the specimen axis

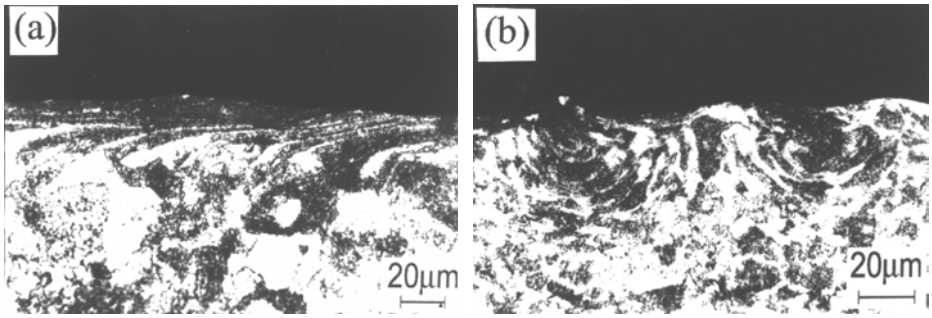

Figure 16: Structure of the surface layer as seen in a longitudinal section for a singularly peened (a) and a double peened (b) specimens.

for singular peened and double peened samples, respectively. Squeezed and refined grains as well as laminar packing of ferrite and pearlite bands almost parallel to the specimen surface are evident.

Examination of the replicas and the sample microsections revealed the main sites of crack initiation. The cracks began to grow from the roots of micropits derived from shot peening or, rarely, from locally damaged zones

on the surface. Figures 17 a, b and 17c, d illustrate surface crack growth patterns on a specimen tested under a shear stress amplitude τa=190 MPa after $N=10^4$ cycles (number of cycles to failure $Nf = 3.4x10^5$). Micrographs in Figure 17 a, b are referred to the singularly peened samples whereas in Figure 17c, d to the double peened ones.

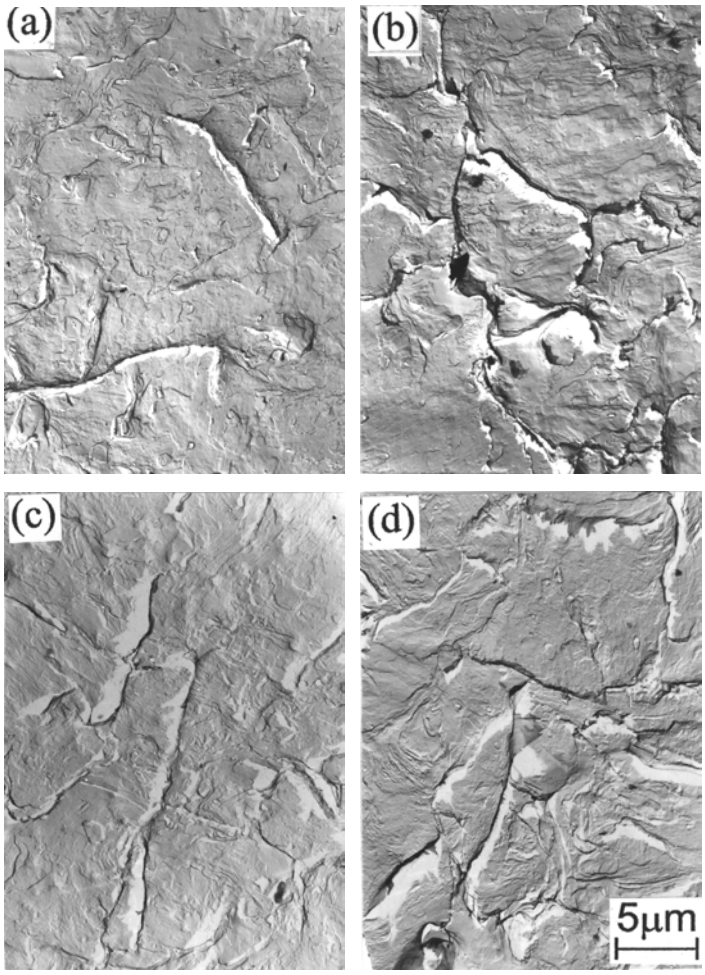

Figure 17: Different systems of the surface short cracks observed for a singularly (a and b) and for a double (c and d) peened samples.

Horizontal edges of the micrographs are parallel to the sample axis. Short cracks have grown from the micropits in various directions but most of which to some extent correspond to directions of shear stresses. Straight

intervals of crack growth path could be related to crack growth in invisible slip bands. Curvilinear intervals of short and long cracks were associated with the development of strongly deformed ferrite grains prior to fatigue testing. Crack depth progress in the samples on a longitudinal section was analysed as well (Figure 18a and b). Its growth was irregular and temporarily arrested at interfaces of the highly deformed bands during the period the crack tunelled along and through the hardened layer. Below that layer the cracks changed their growth direction and extended through the ferrite bands of the matrix material in the conventional manner.

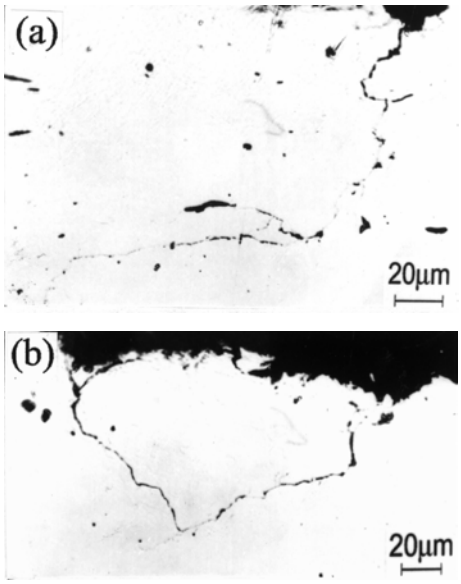

Figure 18: Discontinuous growth of cracks in the depth direction observed on a longitudinal section of a singularly peened (a) and double (b) peened samples.

The mechanism of fracture in the shot peened samples was established from TEM micrographs of the replicas taken from different zones of the fracture surfaces. The micrograph shown in Figure 19a presents the topography of the hardened zone. The micrograph of Figure 19b has been obtained from the border zone between the hardened layer and the matrix. On both fractographs, areas of brittle fracture along cleavage planes can be seen, as well as quasi-cleavage fracture zones with limited plastic deformation symptoms and a zone exhibiting plastic shear deformation. The quasi-cleavage fracture process is found to be predominating type of fracture in the hardened layer

(Figure 19a) and also plastic deformation fracture in the vicinity of the matrix (Figure 19b). The strongly deformed surface layer with a reduced capacity for plasticity due to grain squeezing and a high dislocation density can promote quasi-cleavage fracture. Fatigue striations were only observed in the matrix below the hardened zone that are evident in the lower part of Figure 19 b.

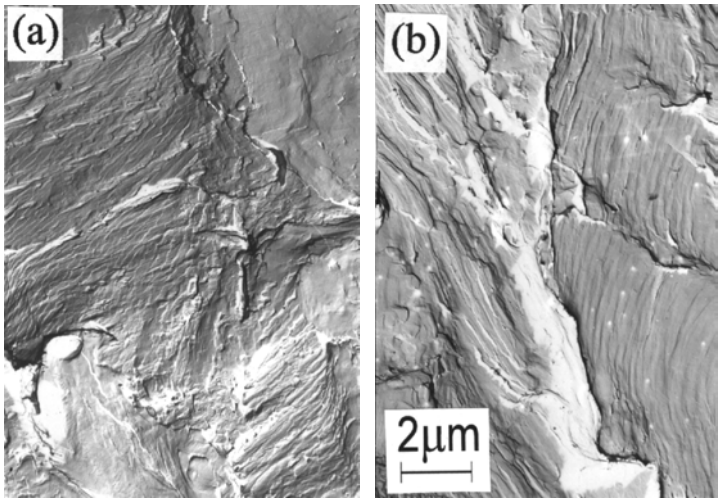

Figure 19: TEM micrographs of a surface fracture derived from (a) the hardened layer and (b) the border zone between surface layer and the matrix.

The numbers of cycles to produce very short fatigue crack growth are greater in peened specimens than in the non-treated samples tested under the same shear stress. This can be attributed to the randomly located sources of crack initiation on the peened specimen surface as well as higher crack opening stress level and high density of dislocations at the grain boundaries. However, in spite of a great number of surface micropits which can act as classical micro-notches for the fatigue specimens both a slower crack growth and a significantly lower crack density were found on the surface of peened samples. These results are bases on both the observations of replicas and analyses of the surface crack growth characteristics carried out for two groups of cracks namely horizontal and vertical cracks seen on the surface bath of which grew individually in directions close to the direction of maximum shear stresses.

The plots of crack advance and growth rate against cycle ratio N_i/N_f in a singularly peened specimens are shown in Figure 20. The shear stress amplitude was τ_a = 190 MPa, N_f = 3.4 X10^5 cycles. These plots could not be drawn for double peened specimens because of high surface deformation and big difficulties with the crack selection in those specimens. The curves illustrating horizontal cracks (with respect to the specimen axis direction) have been denoted as H1 and H2 and the vertical cracks as V1 and V2. The additional curve denoted as AH presents crack growth from a non-treated specimen fatigued at the same stress value. Horizontal cracks have grown mainly from micropits and extended slowly along deformed ferrite bands that are limited by pearlite bands. These microcracks can be called non-propagating cracks because their lengths are only of the order of 500 μm required whole fatigue life for their growth. Vertical cracks were found to initiate in the sites between micropits (type V1) or alternatively to start growing from the roots of micropits (type V2). Shear cracks of the V2 type were temporarily arrested at successive grain bands when passing through the hardened zone. Their growth was fast when they became long cracks. The irregular growth of these cracks is presented in the curves of Figure 20. The vertical cracks V1 began to grow later than type V2 but their growth rates eventually were significantly higher. These V1 type cracks caused

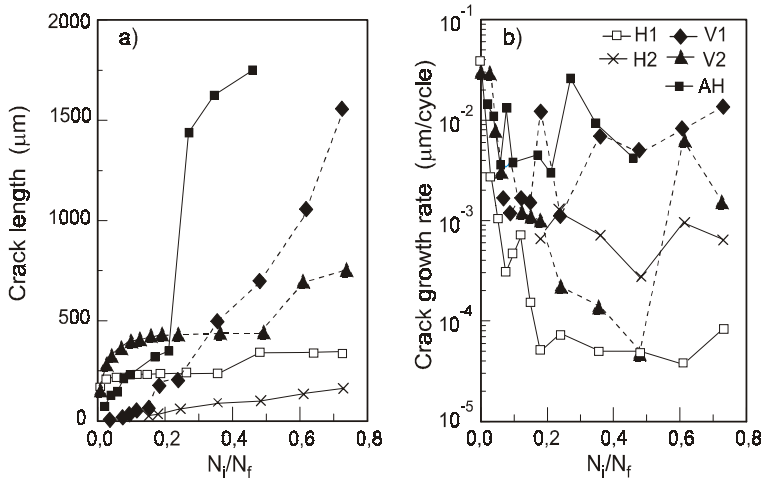

Figure 20: Crack growth behaviour as a function of cycle ratio on (a) crack length and (b) crack growth rate.

failure. The behaviour of the cracks described above differs completely from those in non-peened samples where horizontal cracks grew faster in favourably oriented ferrite bands until failure.

Crack density

A comparative study of surface crack population formed during the fatigue lives of peened and non-treated samples was made with the help of plots drawn on Figure 21. According to the notation for cracks introduced earlier, the symbols H, V, T refer respectively to the population of horizontal cracks, vertical cracks and the total number of cracks found on a unit surface area of the peened specimens. The symbol TA indicates the total number of cracks counted on a non-treated sample at the same shear stress amplitude. The plots show that the crack population in treated specimens is about five times lower and reveals little change during the fatigue life. In peened specimens the influence of crack coalescence on crack growth is small. In opposite the process of crack coalescence plays an important role in crack propagation in non-treated specimens. It is for this reason that the curve TA shows significant fluctuations of crack population against the cycle ratio.

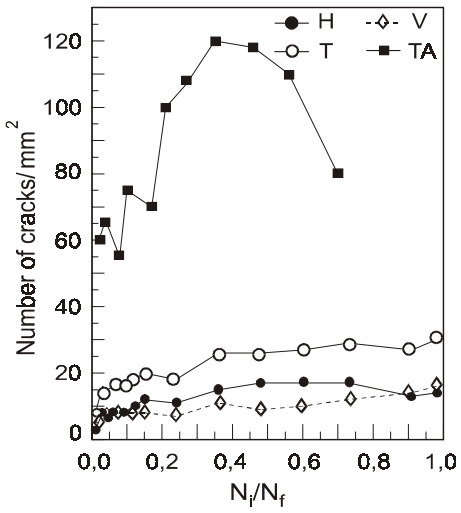

Figure 21: Short cracks population against cycle ratio in a shot peened specimens (curves H,V,T) and in a non-treated specimen (curve TA).

In peened specimens the process of crack initiation and very short crack propagation phases during the prior fatigue and early stage of the specimen life leads to a low population of microcracks of lengths less than 50 μm. (Figure 22a). Their population is a round fifteen times lower than for un-peened samples. As can be seen in Figure 22b the density of longer cracks is low too. As a results of both low crack density and slow crack growth rate in peened specimens the fatigue lives were one and a half time longer in the case of singularly peened specimens and four times longer in the double peened ones than the lives of non-treated samples.

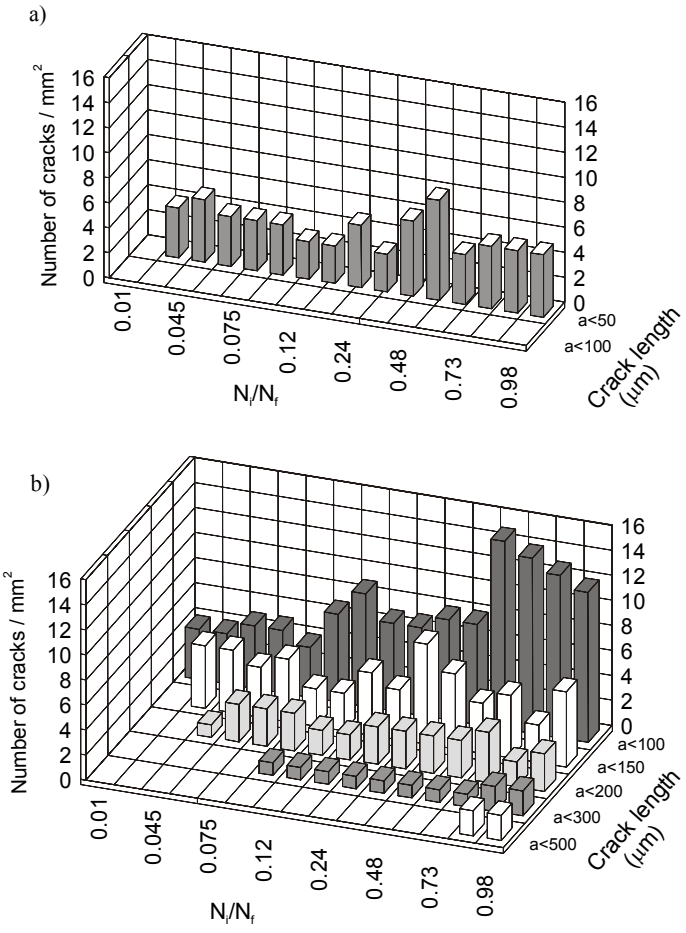

Figure 22: Distribution of cracks length on (a) lower than 50 μm and (b) grater than 50 μm as a function of cycle ratio for a shot-peened specimen.

Summary
Observations of replicas and the examination of microsections of shot peened specimens fatigued under reversed torsion have established several characteristic features of short surface crack growth behaviour [25],[26]. Shot peening can accelerate or retard the phases of crack initiation because of randomly distributed micropits which are mostly the source of crack initiation. Beneficial effect of shot peening is significant mostly in the short crack region and at low cyclic stress levels. Compressive stresses acted in the near surface layer increase the crack opening stress level. Crack growth during the very early stages of fatigue lifetime is slow thus prolonging fatigue life. The initial stage I crack propagation is microstructurally dependent, it means this stage is affected by material surface distorsion. At the same time, the growth rate of cracks during the subsequent crack propagation periods and also the crack density are significantly low. The number of cracks of lengths less than 50 μm was found to be fifteen times lower than in unpeened samples. The reasons are attributed to the great number of barriers in the highly deformed, squeezed grains, the high dislocation density and the compressive residual stresses induced in the hardened layer. Peening residual compressive stresses relax during the loading conditions. This stress relaxation is more rapidly at high cyclic stress and consequently the benefits of peening are more limited. The occurrence of quasi-cleavage fractures involving limited plastic deformation is a characteristic feature of the hardened surface layer. In the matrix below the hardened zone were observed only the fatigue striations.

MODELLING OF SHORT CRACK GROWTH

Characteristic behaviour of crack growth rates in the regime of short crack propagation results from possible crack arrest at grain boundaries and other microstructural barriers. Therefore, crack growth in time consists of passing subsequent barriers with intensity $\lambda(t)$. In the method the fatigue process is regarded as a family of random values of crack length at the related time instances and the crack growth is described by a two-parameter Weibull distribution. This assumption arrive us at the following notation for the crack growth intensity:

$$\lambda(t) = \frac{\delta}{\theta} t^{\delta - 1} \tag{1}$$

where $\delta > 0$ and $\theta > 0$ are the parameters of shape and scale, respectively, of this distribution. Time t in the above and subsequent equations can be expressed by the number of loading cycles. Let an increment Δa in crack length increases in time according with the Paris formula, namely:

$$\Delta a = C\sigma^{m} a^{m} \Delta t \tag{2}$$

Stochastic nature of crack growth is expressed by a function $U_{a,t}$ representing the probability that the crack length is a at the time t. The finite differences equation can be formulated to characterise the dynamics of crack growth:

$$U_{a,t+\Delta t} = \left(1 - \frac{\delta}{\theta} t^{(\delta-1)} \Delta t\right) U_{a,t} + \frac{\delta}{\theta} t^{(\delta-1)} \Delta t \, U_{a-\Delta a,t} \tag{3}$$

where the increment in crack length Δa is defined by equation (2). Transition to functional notation and the Taylor series expansion derives the Fokker-Planck type equation (4):

$$\frac{\partial U(a,t)}{\partial t} = -\frac{\delta}{\theta} t^{(\delta-1)} \cdot \Delta a \, \frac{\partial U(a,t)}{\partial a} + \frac{1}{2} \frac{\delta}{\theta} t^{(\delta-1)} \cdot \Delta a^{2} \, \frac{\partial^{2} U(a,t)}{\partial a^{2}} \tag{4}$$

Function $U(a,t)$ denotes probability density function of a crack length a in time t. Substituting the relation (2) for the increment Δa in the above equation we get its final form:

$$\frac{\partial U(a,t)}{\partial t} = -W \cdot \frac{\delta}{\theta} t^{(\delta-1)} \sigma^{m} a^{n} \, \frac{\partial U(a,t)}{\partial a} + \frac{1}{2} W \frac{\delta}{\theta} t^{(\delta-1)} \sigma^{2m} a^{2n} \, \frac{\partial^{2} U(a,t)}{\partial a^{2}} \tag{5}$$

where $W = C\Delta t$ and $n = m/2$. Integration of the Paris formula in the limits $[a_o, a]$ and $[N_o, N]$, respectively, is the source of the expression for a current crack length a, namely:

$$a = \left[C\sigma^{m}(1-n) \cdot t + a_o^{(1-n)}\right]^{(1/(n-1))} \tag{6}$$

Taking into consideration the initial conditions for short cracks $a_o = 0$ for $t = 0$ then the relation (6) gives the form:

$$a = \left[C\sigma^{m}(1-n)\cdot t\right]^{(1/(n-1))} \tag{7}$$

that after substituting it to equation (5) we can arrive at the following notation for the coefficients $A(t)$ and $B(t)$ appearing in the Fokker-Planck type equation (8):

$$\frac{\partial U(a,t)}{\partial t} = -B(t)\frac{\partial U(a,t)}{\partial a} + \frac{1}{2}A(t)\frac{\partial^2 U(a,t)}{\partial a^2} \tag{8}$$

$$B(t) = W'\frac{\delta}{\theta}\sigma^{m/(1-n)}\cdot t^{[2n+\delta(1-n)-1]/(1-n)} \tag{9}$$

$$A(t) = W'\frac{\delta}{\theta}\sigma^{2m/(1-n)}\cdot t^{[3n+\delta(1-n)-1]/(1-n)} \tag{10}$$

where $W' = 0.5\cdot C^{2/(2-m)}\cdot(2-m)^{m/(2-m)}\Delta t$. A specific solution of equation (8) is found that satisfies the following conditions: for t $\rightarrow$ 0 the solution shows convergence on a Dirac function, i.e. $U(a,t)\rightarrow 0$ for $a \neq 0$ and $U(0,t)\rightarrow +\infty$. Such being the case, it can be shown that solution assumes the form:

$$U(a,t) = \frac{1}{\sqrt{2\pi\int_0^t A(t)dt}}\cdot\exp\left(-\frac{\left(a-\int_0^t B(t)dt\right)^2}{2\int_0^t A(t)dt}\right) \tag{11}$$

Function (11) is a crack length probability density function of Gaussian shape. The parameters of the Gauss distribution, namely $E_t[a]$, σ_t^2 i.e. an average crack length and square standard deviation, respectively, can be calculated in the following way:

$$E[a]_t = \int_0^t B(t)dt = W' \cdot \frac{\delta}{\theta} \frac{2-m}{[m+\delta(2-m)]} \cdot \sigma^{m/(2-m)} \cdot t^{[m+\delta(2-m)]/(2-m)} \quad (12)$$

$$\sigma_t^2 = \int_0^t A(t)dt = W'^2 \cdot \frac{\delta}{\theta} \frac{2-m}{[2m+\delta(2-m)]} \cdot \sigma^{4m/(2-m)} \cdot t^{[2m+\delta(2-m)]/(2-m)} \quad (13)$$

However, the unknown parameters δ and θ have to be estimated on the grounds of experimental data recorded either as length a_i of a crack in time instance t_i or in the form of the number of loading cycles N_i. A possible way of estimation is to make use of a likelihood function. But in this case it will be easier to take advantage of the relations:

$$a_n = W' \frac{\delta}{\theta} \cdot \sigma^{m/(2-m)} \cdot \frac{2-m}{[m+\delta(2-m)]} \cdot t_n^{[m+\delta(2-m)]/(2-m)} \quad (14)$$

$$a_1 = W' \cdot \frac{\delta}{\theta} \cdot \sigma^{m/(2-m)} \cdot \frac{2-m}{[m+\delta(2-m)]} \cdot t_1^{[m+\delta(2-m)]/(2-m)} \quad (15)$$

Transformation of above relations lead to the equality:

$$\frac{a_n}{t_n^{[m+\delta(2-m)]/(2-m)}} = \frac{a_1}{t_1^{[m+\delta(2-m)]/(2-m)}} \quad (16)$$

It can be shown that the unknown parameter δ* gets the following form:

$$\delta^* = \frac{\ln(a_n) - \ln(a_1)}{\ln(t_n) - \ln(t_1)} - \frac{m}{(2-m)} \quad (17)$$

Similarly, transforming equation (14) and equation (15) one gets the expected relations for another parameters:

$$\theta^* = \delta^* \cdot \sigma^{m/(2-m)} \cdot \frac{(2-m)}{[m+\delta^* \cdot (2-m)]} \cdot t_n^{\left[(2m-2)+\delta^* \cdot (2-m)\right]/(2-m)} \quad (18)$$

$$W'^{*} = \frac{l_n}{\frac{\delta^*}{\theta^*}\sigma^{m/(2-m)} \cdot \frac{(2-m)}{\left[m+\delta^* \cdot (2-m)\right]} \cdot t_n^{\left[m+\delta^* \cdot (2-m)\right]/(2-m)}} \tag{19}$$

which are useful if the average crack length $E_t[a]$ and the standard deviation σ_t are calculated. The function $U(a,t)$ gives the grounds for determining the fatigue life from the formula:

$$R(t) = \frac{1}{\sqrt{2\pi}} \int_{-\infty}^{(a_d - E_t[a])/\sigma_t} e^{-z_t{}^2/2} dz \tag{20}$$

Function $R(t)$ denotes the assumed level of probability that the acceptable crack length a_d (in the range of short or long crack) will not be exceeded. The symbol *z* used in this formula denotes a standardised crack length and is defined as follows: $z_t = (a_k - E_t[a])/\sigma_t$.

Implementation of the model

Capability of the probabilistic approach to describe the short crack growth by using the Weibull distribution has been verified taking into consideration experimental data that have been gained for both the circumferentially laser hardened specimens and shot peened ones tested under reversed torsion. Similar diagrams of crack growth rates against crack length and against cycle ratio N_i/N_f have been prepared for dominant cracks detected in the examined specimens.

The plots in Figure 23 reflect dominant cracks grown in the circumferentially laser hardened specimens tested under two stress levels (τ_a = 192, 196 MPa). Continuous lines with filled-in black symbols represent experimental results of crack growth rates da/dN, whereas dashed lines with open (white) symbols show the expected crack growth rates $dE_N[a]/dN$. In Figures 23a and 23b the plots of crack growth rates have been drawn versus crack length and versus cycle ratio N_i/N_f, respectively. Additionally, for any comparison the curve NL related to crack growth rate in non-treated specimen has been plotted in Figure 23a. The results indicate that the effect of surface treatment is particularly visible in the range of short cracks. Crack growth rates are significantly lower in treated specimens. The predicted fa-

tigue lives (up to the acceptable limit a_d in the range of short crack growth) with the probability *R(t)* equal to unity have been estimated for the examined specimens using expression (20). In the case of the specimen tested under stress amplitude τ_a = 192 MPa the calculated lifetime was equalled $N_f^{calc} = 6.9 \cdot 10^4$ cycles and the experimental one was $N_f^{\exp} = 7 \cdot 10^4$ cycles for the assumed acceptable limit a_d = 200 μm. For the second specimen (τ_a=196MPa) the calculated life was $N_f^{calc.} = 2.58 \cdot 10^4$ cycles and the experimental one was $N_f^{\exp.} = 2.5 \cdot 10^4$ cycles for the assumed acceptable limit a_d = 300 μm.

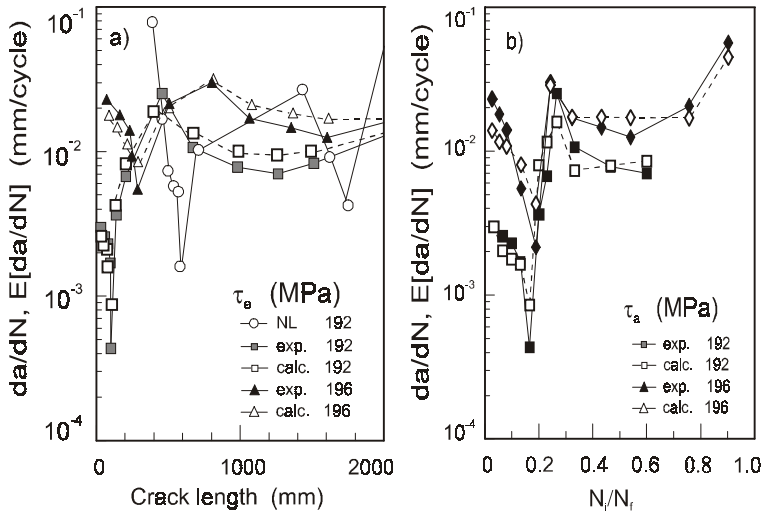

Figure 23: Experimental and calculated plots of crack growth rates against crack length (a) and cycle ratio N_i/N_f (b) in the circumferentially treated specimens tested under different shear stress amplitudes τ_a .

Agreement between the experimental results and the calculated ones can be recognised as pretty good both in terms of the crack growth rates description and the estimation of fatigue life in the range of short crack behaviour.

Exemplary plots of experimentally detected da/dN and calculated crack growth rates $d\,E_N[a]/dN$ versus crack length (Figure 24a, c) and versus cycle ratio N_i/N_f (Figure 24b, d) have been presented for the shot peened specimen tested under stress amplitude τ_a = 190 MPa. The notations used for

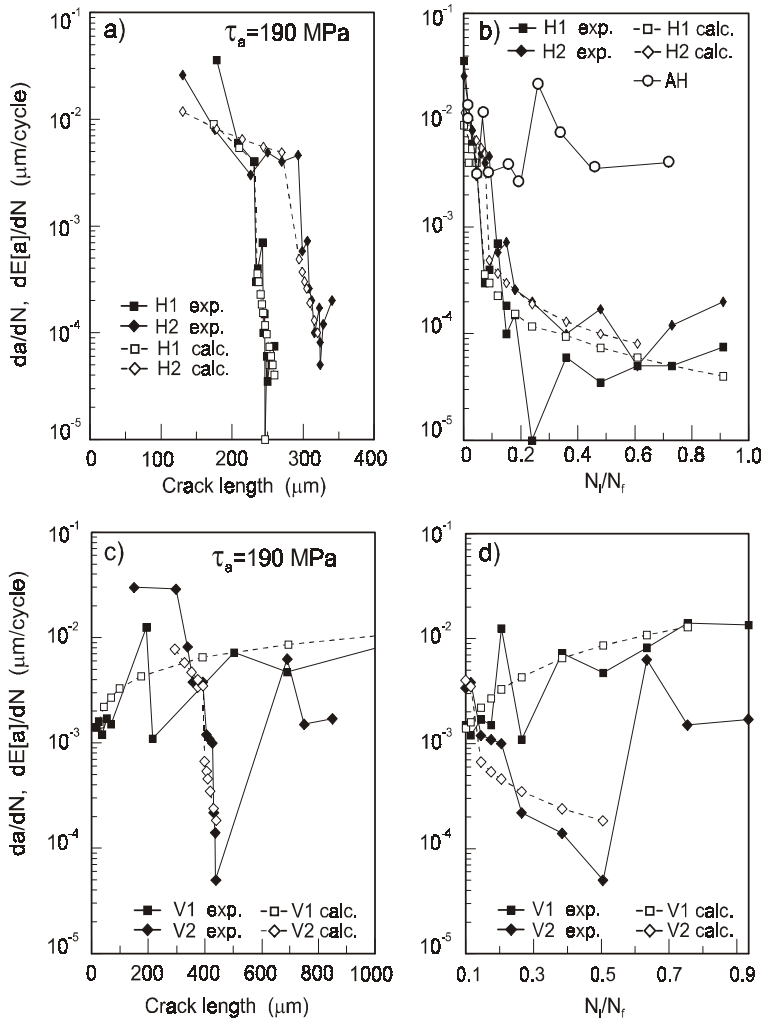

Figure 24: Experimental and calculated plots of crack growth rates against crack length (a, c) and cycle ratio N_i/N_f (b, d) in the shot peened specimen tested under shear stress amplitude τ_a = 190 MPa.

the marks and lines in Figure 24 are similar as in Figure 23. In Figures 24a and 24b the curves are related to the horizontal cracks H1 and H2 developed almost parallelly to the specimen axis whereas the curves in Figures 24c and 24d are referred to the vertical cracks detected in this specimen. Additionally, the curve denoted as AH in Figure 24b illustrates the growth rate of dominant horizontal crack detected in non-treated specimen which was

tested under similar stress level. In normalised specimens the privilege direction of crack growths was the horizontal direction to the specimens axis. The effect of shot peening is particularly visible in the examined specimens. The growth rates of cracks are significantly lower in whole range of crack growth in the treated specimens than in non-treated ones. The calculated curves of crack growth rates predict pretty good the experimental curves recorded in the shot peened specimens.

Summarising the results one can conclude that the probabilistic method presented in the paper facilitates a simplified description of fatigue short crack growth and estimation of fatigue life of the surface treated specimens.

REFERENCES

1. Miller, K.J. and de los Rios, E.R. (1986) Eds. *The behaviour of short fatigue cracks*. EGF (ESIS) Publication 1, Mech. Eng. Publ. , London, U.K.
2. Ritchie, R.O. and Lankford, J. (1986) Eds. *Small fatigue cracks*. TSM-AIME, Warrendale, PA.
3. Miller, K.J. (1999) In: Proc. 7th Int. Fatigue Congress*, Fatigue'99*, Beijing, China, X.R. Wu and Z.G. Wang (Eds). EMAS U.K. and Higher Education Press China, 1999, Vol. 1/4, pp. 15-40.
4. Ritchie, R.O. (1999) Ibidem, Vol. 1/4, pp. 3-14.
5. Miller, K.J. (1997) STP 1296, ASTM Philadelphia, pp. 267-286.
6. Vasudevan, A.K., Sadananda, K. and Louat, N. (1994) *Journal of the Material Sciences and Engineering*., A 188, pp. 1-22.
7. McEvily, A.J. and Ritchie, R.O. (1998) *Journal of Fatigue and Fracture of Engng Materials and* Structures*,* Vol. 21, No 7, pp. 847-855
8. Jono, M. and Sugeta, A. (1996) *Journal of Fatigue and Fracture of Engng Materials and* Structures*,* Vol. 19, No 2/3, pp. 165-174.
9. Halliday M.D., Poole P and Bowen P. (1995) *Ibidem*, Vol. 18, No 6, pp. 717-730.
10. Tokaji K, Ogawa T. (1992) In: *Short Fatigue Cracks*, ESIS Publication 13, K.J. Miller and E.R. de los Rios (Eds), London, pp. 85-99.
11. Petit J., Kosche K. (1992) I*bidem*, pp. 135-151.
12. Reed P.A., King J.E. (1992) *Ibidem*, pp. 153-168.
13. Wu X.J., Akid R. (1995) *Journal of Fatigue and Fracture of Engng Materials and* Structures, Vol. 18, No 4, pp. 443-454.

14. Hussey I.W., Byrne J., Locke W. (1992) In: *Short Fatigue Cracks*, ESIS Publication 13, K.J. Miller and E.R. de los Rios (Eds), London, pp. 305-318.
15. Ahmad H.Y., de los Rios E.R., Yates J.R. (1994) *Journal of Fatigue and Fracture of Engng Materials and* Structures, Vol. 17, No 2, pp. 235-242.
16. Hong Y., Qiao Y., Liu N., Zheng X. (1999) In: Proc. 7th Int. Fatigue Congress, Fatigue'99, X.R. Wu, Z.G. Wang (Eds), Beijing, China, Vol1/4, pp. 337-344.
17. Kocańda, D. and Kocańda, S. (1996) *Journal of Theorethical and Applied Mechanics*, Vol. 34, No 2, pp. 327-343.
18. Choi H.C., Song J.H. (1995) *Journal of Fatigue and Fracture of Engng Materials and* Structures, Vol. 18, No 1, pp. 105-117.
19. Kocańda, S. and Natkaniec, D. (1992) *Ibidem,* 1992, Vol. 15, No 12, pp. 1237-1249.
20. Kocańda, S. and Natkaniec, D. (1992) In: Proc. 2nd Int. Conf. Computer Aided Assessment and Control. *Localized Damage'92*, Southampton, U.K., Elsevier Appl. Science, Vol. 1, pp. 549-563.
21. Natkaniec, D., Kocańda, S. and Miller, K.J. (1994) *Journal of Theorethical and Applied Mechanics*, Vol. 32, Nr 1, pp. 163–176.
22. Natkaniec D., Kocańda S. and Miller K.J. (1994) In: Structural Integrity, Experiments-Models-Applications. Proc. of the *10th Biennial European Conf. on Fracture, ECF10*, Berlin, Germany, 1994, EMAS U.K., Vol. II, pp. 1259–1264.
23. de los Rios E.R., Mercier P., El-Sehily, B.M. (1996) *Journal of Fatigue and Fracture of Engng Materials and* Structures, Vol. 19, No 2/3, pp. 175-184.
24. Sharp P.K., Liu Q, Barter S.A., Baburamani P. and Clark G. (2002) *Ibidem*, Vol. 25, No 2, pp. 99-110.
25. Kocańda, D. and Kocańda, S. (1995) In: 1st Workshop on Influence of Local Stress and Strain Concentrators on the Reliability and Safety of Structures. Copernicus Network Program. Miskolc, Hungary, pp. 158-167.
26. Kocańda, D. and Kocańda, S. and Miller K.J. (1995) *Journal of Fatigue and Fracture of Engng Materials and* Structures, Vol. 19, No 7, pp. 911-917.